

# MeerCRAB: MeerLICHT Classification of Real and Bogus Transients using Deep Learning

Zafirah Hosenie<sup>1\*</sup> · Steven Bloemen<sup>2</sup> · Paul Groot<sup>2,3,4</sup> · Robert Lyon<sup>5</sup> · Bart Scheers<sup>6</sup> · Benjamin Stappers<sup>1</sup> · Fiorenzo Stoppa<sup>2</sup> · Paul Vreeswijk<sup>2</sup> · Simon De Wet<sup>3</sup> · Marc Klein Wolt<sup>2</sup> · Elmar Körding<sup>2</sup> · Vanessa McBride<sup>3,7</sup> · Rudolf Le Poole<sup>8</sup> · Kerry Paterson<sup>9</sup> · Daniëlle L. A. Pieterse<sup>2</sup> · Patrick Woudt<sup>3</sup>

Accepted: 22 April 2021

**Abstract** Astronomers require efficient automated detection and classification pipelines when conducting large-scale surveys of the (optical) sky for variable and transient sources. Such pipelines are fundamentally important, as they permit rapid follow-up and analysis of those detections most likely to be of scientific value. We therefore present a deep learning pipeline based on the convolutional neural network architecture called MeerCRAB. It is designed to filter out the so called “bogus” detections from true astrophysical sources in

the transient detection pipeline of the MeerLICHT telescope. Optical candidates are described using a variety of 2D images and numerical features extracted from those images. The relationship between the input images and the target classes is unclear, since the ground truth is poorly defined and often the subject of debate. This makes it difficult to determine which source of information should be used to train a classification algorithm. We therefore used two methods for labelling our data (i) thresholding and (ii) latent class model approaches. We deployed variants of MeerCRAB that employed different network architectures trained using different combinations of input images and training set choices, based on classification labels provided by volunteers. The deepest network worked best with an accuracy of 99.5% and Matthews correlation coefficient (MCC) value of 0.989. The best model was integrated to the MeerLICHT transient vetting pipeline, enabling the accurate and efficient classification of detected transients that allows researchers to select the most promising candidates for their research goals.

**Keywords** methods: data analysis · methods: deep learning · techniques: image processing, surveys · stars: general, transients: real, bogus

## 1 Introduction

Contemporary large-scale optical surveys such as Skymapper (Keller et al. 2007), the Palomar Transient Factory (PTF, Rau et al. 2009), the Catalina Real-time Transient Survey (CRTS, Drake et al. 2009), the Panoramic Survey Telescope and Rapid Response System (Pan-STARRS1, Kaiser et al. 2010), the All-Sky Automated Survey for SuperNova (ASASSN, Shappee et al. 2014), Gaia (Gaia Collaboration et al. 2016), the MeerLICHT telescope (Bloemen et al. 2016; Paterson 2019) and the Zwicky Transient Factory (ZTF, Bellm et al. 2019) are generating a plethora of transient

<sup>1</sup>Jodrell Bank Centre for Astrophysics, Department of Physics and Astronomy, The University of Manchester, Manchester M13 9PL, UK. E-mail: zafirah.hosenie@gmail.com

<sup>2</sup>Department of Astrophysics/IMAPP, Radboud University, P.O. 9010,6500 GL, Nijmegen, The Netherlands.

<sup>3</sup>Inter-University Institute for Data Intensive Astronomy & Department of Astronomy, University of Cape Town, Private Bag X3, Rondebosch 7701, South Africa.

<sup>4</sup>South African Astronomical Observatory, P.O. Box 9, 7935 Observatory, South Africa.

<sup>5</sup>Department of Computer Science, Edge Hill University, Ormskirk Lancashire L39 4QP, UK.

<sup>6</sup>Dataspex B.V., c/o Centrum Wiskunde & Informatica, PO Box 94079, 1090 GB Amsterdam, The Netherlands.

<sup>7</sup>IAU-Office For Astronomy for Development, P.O. Box 9, 7935 Observatory, South Africa.

<sup>8</sup>Leiden Observatory, Leiden University, P.O. Box 9513, NL-2300 RA Leiden, The Netherlands.

<sup>9</sup>Center for Interdisciplinary Exploration and Research in Astrophysics (CIERA) and Department of Physics and Astronomy, Northwestern University, Evanston, IL 60208, USA.

events originating from a wide range of sources. These instruments enable us to observe and explore changes in millions of sources/candidates, thus unlocking new opportunities for interpreting and understanding large families of sources.

The MeerLICHT facility provides a 2.7 square degree field-of-view at a pixel scale of 0.56"/pixel (Bloemen et al. 2016) that maximises the volume of astrophysical candidates with brightnesses appropriate for spectroscopic follow-up using current large-aperture optical facilities. More details regarding the survey can be found in Bloemen et al. (2016). Both MeerLICHT and the BlackGEM array (Groot 2019) (that is currently being installed at the La Silla Observatory in Chile) will yield about 500 observations per night, per telescope, thus generating hundreds of candidate alerts every clear night that could be spectroscopically followed up. BlackGEM’s main focus is on the detection of optical counterparts to gravitational wave events and MeerLICHT is used to co-observe the sky as seen with the MeerKAT radio array (Jonas & MeerKAT Team 2016). MeerLICHT and BlackGEM are technically identical with MeerLICHT being the prototype for the BlackGEM array.

Transients and variables are sources that vary on all timescales (from milliseconds up to years) and they vary significantly from a reference image - either an increase or decrease in brightness. Transients include phenomena such as supernovae, gamma-ray bursts, tidal disruption events and flare stars, to name a few. A successful transient follow-up program enables the creation of a large database of transient and variable sources. Such large databases are important for future analyses of data collected during upcoming photometric surveys such as those conducted at the Vera C. Rubin observatory (LSST; LSST Science Collaboration et al. 2009). While we possess a reasonable understanding of many transient sources, achieved via consideration of their spectra, the main goal of surveys undertaken with MeerLICHT is to find and select the subset of sources that are not well understood. This will help us to increase our knowledge of the different families of transients and variable stars. Secondly, given that transients are rapidly fading sources due to their often destructive nature, MeerLICHT aims to identify transients rapidly, as they are only visible for a limited amount of time for follow-up.

In order to have an early and rapid characterisation of these sources, it is fundamentally important to automate several steps within a transient detection pipeline, including the separation of transients/astrophysical events from “bogus” detections, which has become a bottle-neck in fast detection pipelines. So called “bogus” detections can occur as a result of saturated sources, convolution problems, defects in the detector, atmospheric dispersion, unmodeled differences at the subtraction stage and cosmic rays passing through the detector, amongst other things.

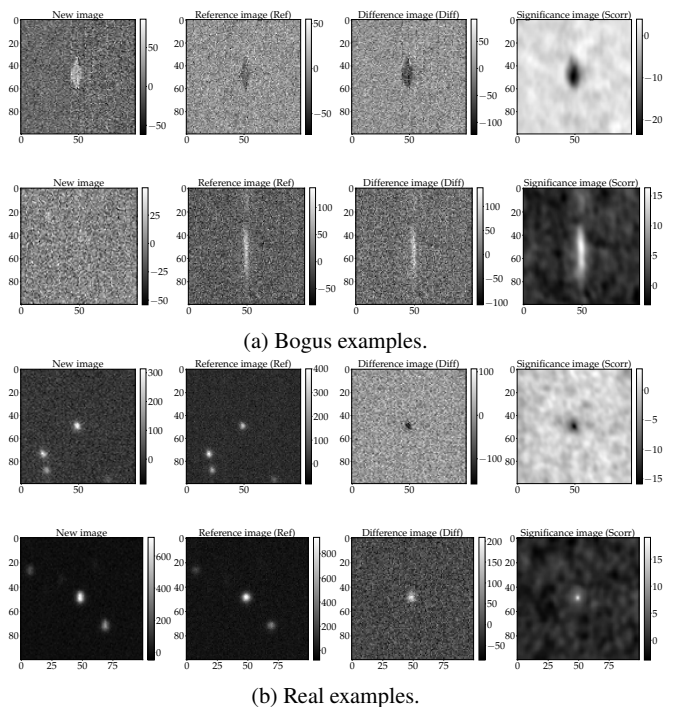


Fig. 1: Examples of bogus and real transients in the MeerLICHT database. Each column represents the new (N), reference (R), difference (D) and significance (S) images and the rows are the different fields.

Most surveys use three images for transient event detection and extraction: (i) an early observation of the relevant sky (also known as the *template/reference* image), (ii) a calibrated recent image (*New/Science* image), (iii) the *difference* image which is formed by subtracting the *reference* image from the *new/science* image. Using the difference image, one can, in principle, effectively detect transients, however, in many cases, the subtracted image contains bogus sources.

Therefore to be successful, surveys require an automated way to distinguish between real and bogus candidates. To address this challenging task, most of the time-domain surveys mentioned previously have adopted machine learning (ML) algorithms to perform real-bogus classification. Convolutional neural networks (CNNs, Lecun et al. 1999) have been used in the image domain as feature extractors for automatic vetting algorithms, for example, during the Skymapper Survey (Gieseke et al. 2017), the High cadence Transient Survey (HiTS, Cabrera-Vives et al. 2017) and the ZTF (Bellm et al. 2019) similarly utilized deep learning techniques. Other ML techniques such as Random Forest (RF) and  $k$ -Nearest Neighbour ( $k$ -NN) classification approaches have been employed to classify light curve transients from CRTS (Richards et al. 2011; Hosenie et al. 2020, 2019).

The classification task in these surveys is usually separated into two distinct steps. Firstly, bogus candidates are fil-

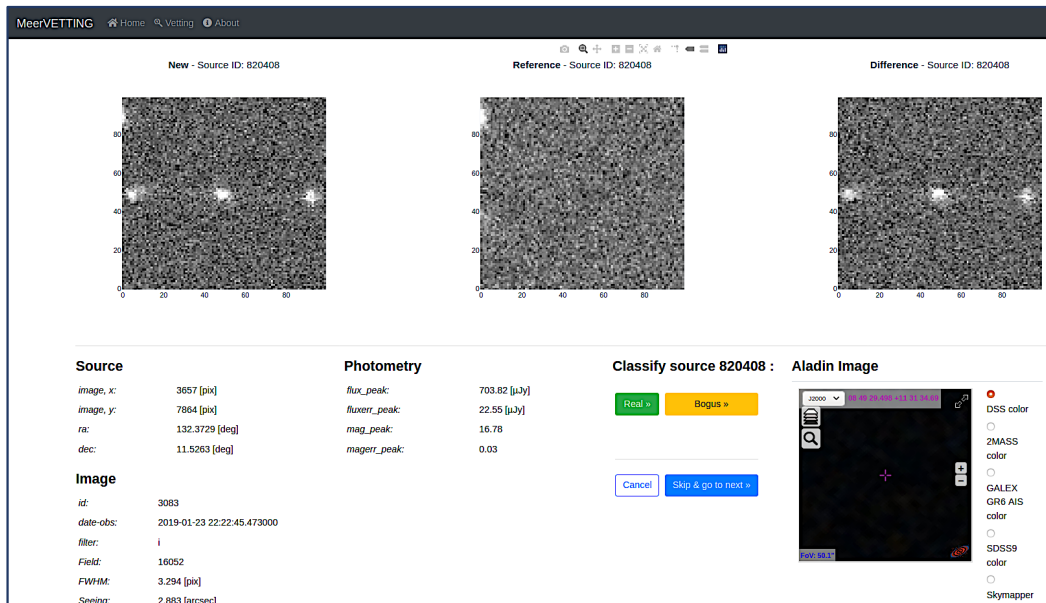


Fig. 2: MeerVETTING web-interface used to label MeerLICHT candidates as either real, bogus or skip confused candidates. Vettors are provided with three images (new, reference, difference) that are cut-outs of the science images.

tered out from real sources immediately after acquiring data, that is, the classification between real and bogus. The second stage involves assigning an astrophysical category/class label to each detected transient based on its spectroscopic or photometric information (e.g. Muthukrishna et al. 2019). In this paper, we focus on the automation of the first stage, that is, the classification of sources as either Real or Bogus using deep learning methods developed for the MeerLICHT facility.

We note that when using ML based automated classification systems, we should not use models trained on data acquired at one telescope, to make predictions upon data acquired by another. Doing so constitutes a violation of the i.i.d principle, which ultimately limits classification performance and consistency. In addition, labelling mistakes are often even more costly - especially on rare sub-classes of transient phenomena. The performance of an ML system is thus entirely dependent upon the quality and distributional properties of the input data and the associated labels it is given. For a system to perform well for a given task, it must be built using data and labels that are distributionally similar to the data it must process in practice. In this work, we present two labelling strategies to label our data (i) *thresholding* which removes noisy labelling and (ii) the *Latent class model*,  $L_{lcm}$  (Formann 1984) which incorporates labelling uncertainty in our model. Afterwards, we constructed three models based on CNNs to build a new robust system that separates real candidates from their bogus counterparts for the MeerLICHT-transient search pipeline. In §2 we provide an overview of the MeerLICHT telescope and we detail the

data used for training and testing the MeerCRAB algorithms. In §3, the methods, network set-up and architectures are described. Results and experimental set-up are detailed in §4, followed by our main conclusions in §5.

## 2 The MeerLICHT facility

MeerLICHT is an optical wide-field telescope that is operated robotically. The telescope is located at the Sutherland station of the South African Astronomical Observatory (SAAO). It consists of a 65 cm primary mirror and provides a 2.7 square degree field-of-view at a pixel scale of  $0.56''/\text{pixel}$  (Bloemen et al. 2016). MeerLICHT will co-observe with the MeerKAT radio telescope on the same field. The combination of an optical and a radio telescope will enable the study of fast transient phenomena using simultaneous observations in two very distinct parts of the electromagnetic spectrum, whilst eliminating the delay introduced by triggering optical follow-up after the detection of a radio event.

MeerLICHT (and also BlackGEM) images are processed by the BlackBOX package<sup>1</sup> to produce image products and catalogs of all objects detected as well as transient candidates resulting from optimal image subtraction. The raw MeerLICHT images are automatically transferred from SAAO to the Inter-university Institute for Data Intensive Astronomy (IDIA<sup>2</sup>) in Cape Town, South Africa, and processed by BlackBOX.

<sup>1</sup> see <https://github.com/pmvreeswijk/BlackBOX> and <https://github.com/pmvreeswijk/ZOGY>

<sup>2</sup> see <https://www.idia.ac.za/>

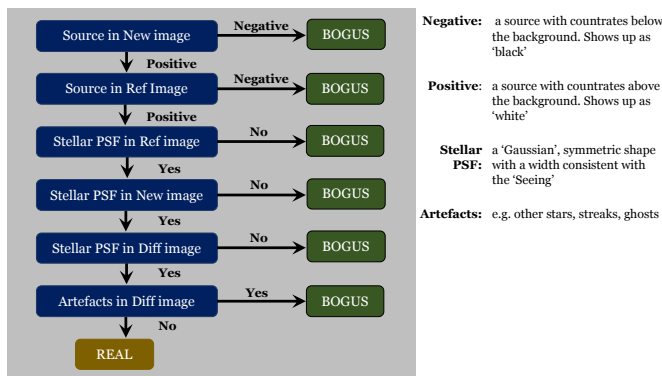


Fig. 3: Decision tree characterising real and bogus candidates. Vettors used this guide to label each candidate and to construct a large training set for MeerCRAB.

First, the images are gain and overscan-corrected, and flatfielded using a set of twilight flats. Cosmic rays and satellite trails are detected using the astrocrappy<sup>3</sup> implementation of LA Cosmic (van Dokkum 2001) and STSDAS satdet<sup>4</sup> modules, respectively. Subsequently, the following steps are performed: object detection using Source-Extractor (Bertin & Arnouts 1996), astrometric calibration using Astrometry.net (Lang et al. 2010), estimation of the Point Spread Function (PSF) as a function of position using PSFEx (Bertin 2011) and photometric calibration. The latter is done using a custom-built catalog of calibration stars in the MeerLICHT photometric system based on fitting stellar spectral templates to Gaia, SDSS, PanSTARRS, SkyMapper, 2MASS and GALEX photometry.

Finally, optimal image subtraction is performed, comparing the new image with a reference image, closely following the prescriptions of Zackay, Ofek & Gal-Yam, a.k.a. ZOGY (Zackay et al. 2016). To allow for the PSF to vary across the image, the full MeerLICHT images are divided into 8 by 8 subimages, on which the ZOGY calculations are applied separately, before inserting the subimages back into a full image. The following images are produced: a difference ( $D$ ) image (see Eq. 13 in the ZOGY paper) and a statistics (also known as significance /  $Scorr$ ,  $S$ ) image (see Eqs. 16 and 17 in the ZOGY paper) providing the probability of a transient being present at a particular position. The  $Scorr$  image,  $S$ , is normalized by the Poisson noise of the input images and the error resulting from the astrometric uncertainty when remapping the reference image to the new image frame; this leads to the  $Scorr$  image (see Eq. 25 in the ZOGY paper), which we also refer to as the significance image. The unit of this  $Scorr$  image is standard deviations (sigma) and transients above an adopted significance threshold (we used  $Scorr \geq 12$  for the data presented in this paper) are normally selected on the

basis that they are potentially significant. In practice, many significant but artificial transients are present in collected data due to cosmic rays, saturated stars, bad pixel regions or other image artefacts; many of these can be filtered out with some basic constraints applied to the size and shape, but for each image, tens of transient candidates remain where we only expect a few astrophysical transients per image.

The MeerLICHT/BlackGEM database ingests the transient catalogs produced by BlackBOX, including  $1 \times 1$  arcminute thumbnail cut-outs around each transient of the new ( $N$ ), the reference ( $R$ ), the difference ( $D$ ) and significance /  $Scorr$  ( $S$ ) image as shown in Figure 1. The process of creating a training set for MeerCRAB is detailed in the next section.

## 2.1 MeerLICHT dataset and data labelling

Our goal is to automate the separation of real candidates from bogus objects for the MeerLICHT transient detection pipeline. The main challenge faced when building a supervised automated system is that we need to construct a large labelled data set that can be used to train a ML model. In addition, the data set needs to be representative, that is, we should have a fairly balanced number of real and bogus candidates. If the latter are unavailable, ML algorithms built from such unrepresentative data tend to be biased towards the majority class (e.g. Hosenie et al. 2019).

We therefore construct a large representative training dataset for the Real-Bogus challenge by manually vetting a selection of transients, using a web-interface, known as MeerVETTING as shown in Figure 2. Using the MeerLICHT database, a set of 5000 transient candidates were randomly selected from MeerLICHT data taken between 2017 and 2020. A team of 10 people ("vettors") were presented with three  $100 \times 100$  pixels images during vetting, i.e. the new ( $N$ ), reference ( $R$ ), and difference ( $D$ ). The properties for real and bogus candidates were defined as a phenomenological distinction based solely on the MeerLICHT data, not an astrophysical distinction. In the context of MeerLICHT data, 'positive' implies positive pixel values and 'negative' points to negative pixel values located at the centre of the  $100 \times 100$  images.

- Real is any source that is of astrophysical origin, and variable in time and/or position. A real source therefore
  1. has a shape that reflects a point-source. Most MeerLICHT data is taken in decent focus conditions, so it implies that the source is round, and has a (visual) extent of  $\sim 5$ -10 pixels,
  2. is positive in either the new or the reference image,
  3. can be variable in both directions, e.g. fading or brightening between the new and reference image,

<sup>3</sup> see <https://github.com/astrophy/astrocrappy>

<sup>4</sup> see <https://acstools.readthedocs.io/en/latest/satdet.html>

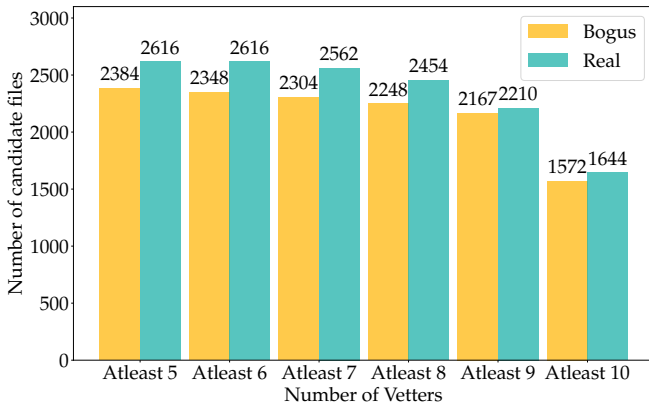


Fig. 4: Thresholding method used to analyse the labelling provided by vetters. The x-axis represents criteria we applied on the labelling. For *Atleast 9 (T9)*, this indicates that 9 out of the 10 vetters have agreed on the labelling. Similar strategy applies for *Atleast 5 (T5)* to *Atleast 10 (T10)*. The y-axis is the number of candidates with a given label, either real or bogus.

and is therefore positive or negative in the difference image and the significance image,

4. can (dis)appear between the new and the reference image. This means that in one of the two images there is no source at all, and in the other there is a clear point-source.
- Bogus is any source that is not of astrophysical origin. A bogus source therefore generally has
    1. a shape that is not a point-source: not round, not ‘Gaussian’, with a size  $\leq 5$  pixels or  $\geq 10$  pixels,
    2. is negative in the new image,
    3. is positive in the new image but negative in the reference image.

Before using the MeerVETTING web-interface, vetters were provided with a visual guide of the various properties of real and bogus candidates. By providing vetters with a guide, we in principle create better annotators, who should produce better labels which in turn should yield improved ML models - as long as the guide itself is not inherently biased in some way. The above characteristics are summarised in a decision-tree as shown in Figure 3. Using the MeerVETTING web-interface, vetters based their decision to manually vet a source as either Real or Bogus by following the decision-tree.

Despite these guidelines, the decision is still subjective whilst there remain boundary cases that are hard to label. Therefore large training datasets will almost always contain examples with inaccurate labels. We test the performance of the MeerCRAB models by (i) removing confused candidates (noisy labels) using a *thresholding* method, and (ii) including the entire dataset with labels based on the latent class model,

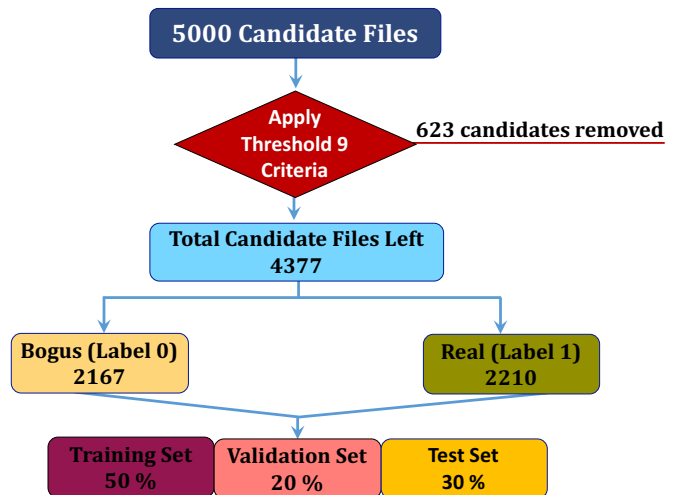


Fig. 5: An example of the procedure for selecting the candidates for training the CNN using the thresholding approach, applied on the 5000 candidates. In this example, *Atleast 9 (T9)* is applied and we note that 623 candidates are discarded. Then, the remaining candidates (4377) are split into training, validation and test set for training and evaluation processes.

$L_{lcm}$ . In the following sections, we provide a brief discussion of the two methods.

## 2.2 Labelling data with Thresholding Method

Our sample of real-bogus training samples is constructed from a pool of 5000 candidates that has been selected randomly. Each object is classified by 10 vetters as either real, bogus or can be skipped if they are unsure how to classify it. Each vetter’s ability to classify a particular candidate may vary according to the class, images, criteria and experience. This may result in very different classifications for the same candidate. We therefore assign a probability  $\mathcal{P}(Real)$  and  $\mathcal{P}(Bogus)$  to each vetted candidate as follows:

$$\mathcal{P}(Real) = \frac{n(R)}{n(T)}, \quad (1)$$

$$\mathcal{P}(Bogus) = \frac{n(B)}{n(T)}, \quad (2)$$

where  $n(R)$  is the total number of vetters who classified a candidate as real,  $n(B)$  is the total number of vetters who classified a candidate as bogus,  $n(T)$  is the total number of vetters classifying a particular candidate and in this case  $n(T) = 10$  as none of the vetters skipped a particular candidate. The vetters classification results are illustrated in a bar plot as shown in Figure 4. If a candidate has  $\mathcal{P}(Real) \geq 0.9$ , it will be given the label real or if  $\mathcal{P}(Bogus) \geq 0.9$ , it will

be assigned as bogus in the bar plots with x-axis “Atleast 9” (T9). Each bar corresponds to a threshold, e.g, the last bar indicates that out of 5000 candidates, 3216 labelled objects are agreed upon by all the 10 vetters, of which 1572 are bogus and 1644 real. Therefore, there are 1784 sources remaining for which vetters did not agree completely and these confused candidates are removed from the data when using T10. In the “Atleast 9” (T9) case, there are 2167 sources where vetters agreed they are bogus and 2210 sources where “Atleast 9” vetters say they are real, and so on. Going down to T5, that is, “Atleast 5” vetters where all the 5000 candidates have been assigned a class, with 2384 bogus and 2616 real. In this paper, we will analyse what happens to the classification results when varying thresholds from T8 to T10.

### 2.3 Labelling data with Latent Class Model, $L_{lcm}$

Latent class model (LCM) is a statistical technique used to classify candidates into mutually exclusive, or latent classes. When data is in the form of a series of categorical responses, for example individual-level voting data as in the case of real-bogus classification, it is often an interesting technique to identify and characterize clusters of similar cases. In this paper, some confused sources<sup>5</sup> were removed from the data when using the *thresholding* method as shown in Figure 5. The process outlined in Figure 5, is exactly the same irrespective of the threshold used, the only difference lies in the number of candidates removed when the threshold is applied. However, these confused sources are useful for determining how the system will perform in a real-world scenario. Therefore, confused examples will also be used during the evaluation phase, and this is achieved by using  $L_{lcm}$  to assign them their most likely labels. Therefore, for the  $L_{lcm}$  technique we used all 5000 candidates during the training and evaluation phase.

LCM relates a set of observed multivariate variables to a set of latent variables. The latent variable is usually discrete. A class is identified by a pattern of conditional probabilities that provide the chance that variables are given certain values.

Let us take the situation of real versus bogus, we want to use LCM to understand the labels provided by the vetters and give a final label to each source. Imagine that class 0-1 is given to a range of candidates with characteristics a, b, c, and d and that class 0 is associated with the presence of characteristics a, b, and c, and class 1 with characteristics b, c and d. LCM will try to detect the presence of latent classes (the candidates entities), generating patterns of association in the characteristics. Then LCM is used to classify candidates according to their maximum likelihood class membership.

The introduction of a latent variable ensures conditional independence within each latent class, the observed vari-

ables, in this case the vetters’ labelling, are statistically independent. The association between the observed variables is explained by the classes of the latent variable (McCutcheon 1987).

The latent class model can be formulated as follows:

$$\mathcal{P}_{i_1, i_2, \dots, i_N} \approx \sum_c \mathcal{P}_c \prod_n \mathcal{P}_{i_n, t}^n, \quad (3)$$

where  $C$  is the number of latent classes and in our case,  $C = 2$ , i.e. real and bogus classes.  $N$  is the number of observed binary variables (in this case,  $n = 1, \dots, 10$ , since we have 10 vetters) and  $\mathcal{P}_c$  are the unconditional probabilities that should sum to one.  $\mathcal{P}_{i_n, t}^n$  are the marginal/conditional probabilities.

### 3 MeerCRAB: A Real-Bogus Intelligent Distinguisher for the MeerLICHT facility using Deep Learning

Before providing further details on the model used, we define a few important terms that will be used in this paper. We labelled bogus examples as 0 and real examples as 1, therefore,

- TP: true positives are real candidates correctly classified as real,
- TN: true negatives are bogus candidates correctly classified as bogus,
- FP: false positives are bogus candidates that are classified as real,
- FN: false negatives are real candidates that are classified as bogus.

From the above definition, our classifier must minimize the number of FP and FN. This is because we do not want to lose many real candidates falsely classified as bogus (FN) and we want to minimize contamination (FP) by any bogus candidates in our final sample.

To overcome this challenge, we employed a Convolutional Neural Network as it has been proven by various studies to have excellent classification performance (Gieseke et al. 2017; Cabrera-Vives et al. 2017; Bellm et al. 2019; Vafaei Sadr et al. 2019; Lin et al. 2020). In this work, we construct three CNN models, referred to as MeerCRAB1, MeerCRAB2, and MeerCRAB3. The details of the CNN models are illustrated in Figure 6. MeerCRAB1 is a network with a single convolutional layer (CL), MeerCRAB2 comprises two CLs while MeerCRAB3 is a deeper network with three CLs. Each CL is made of  $(3 \times 3)$  pixel filters, together with a Rectified Linear Unit (ReLU, Agarap 2018) function, followed by a pooling layer with filter size of  $(2 \times 2)$ . After the CLs, we used fully connected layers (also known as dense layers). In addition, we use a dropout rate varying from (0.1 to 0.5) after each of the pooling and dense layers as seen in Figure 6

<sup>5</sup> 5 vetters labelled them as bogus and the other 5 as real.

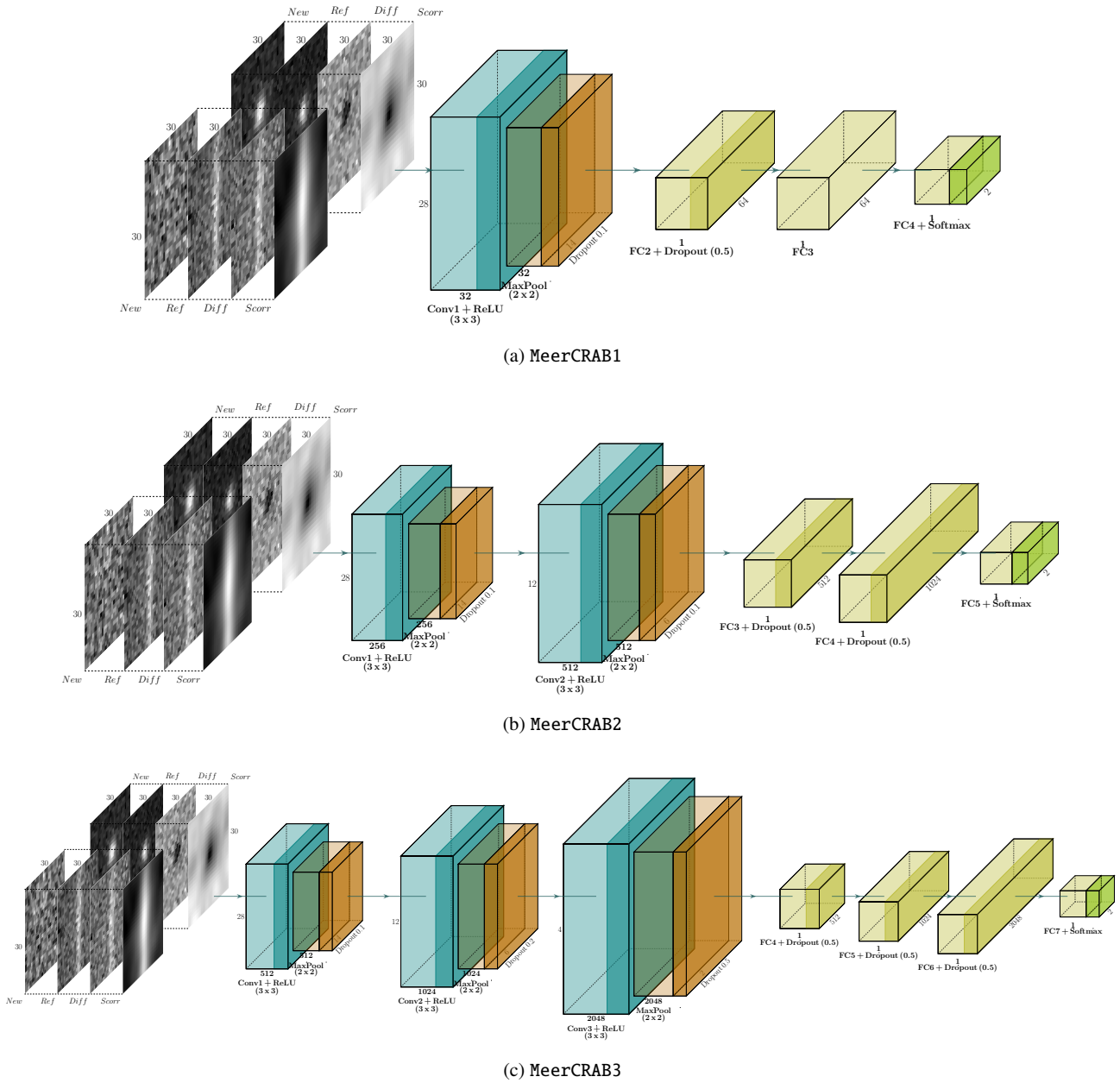


Fig. 6: The three network architectures considered in this work: MeerCRAB1, MeerCRAB2 and MeerCRAB3. We show four images grouped together (new, reference, difference and significance) to form the input of the networks, followed by convolutional layers, max-pooling, dropout and dense layers. At the end, the network outputs a probability whether a candidate is either real or bogus during the prediction phase.

to avoid over-fitting. For the output layer, we used a softmax function that outputs a probability value between 0 and 1.

The implementation of MeerCRAB is made using the TensorFlow<sup>6</sup> and Keras (Chollet & others 2018) API with Python v3.6. For training the MeerCRAB models, we used an Nvidia GeForce GTX 1080Ti 11GB GPU. During training, the binary cross-entropy loss function, Adam optimizer

(Kingma & Ba 2014) with a low learning rate ( $\text{lr} = 0.0002$ ) and a batch-size of 64 were used. We then split our data for each and every experiment as follows: 50% training, 20% validation and 30% testing. As input to the MeerCRAB models, we cropped the  $(100 \times 100)$  pixel images that were analysed by vetters to  $(30 \times 30)$  pixel images. We also utilized the  $(100 \times 100)$  pixel images during training, but we observed a drop in performance and therefore only use the  $(30 \times 30)$  pixel images cropped from the centre. This pre-processing

<sup>6</sup> <https://github.com/tensorflow/tensorflow>

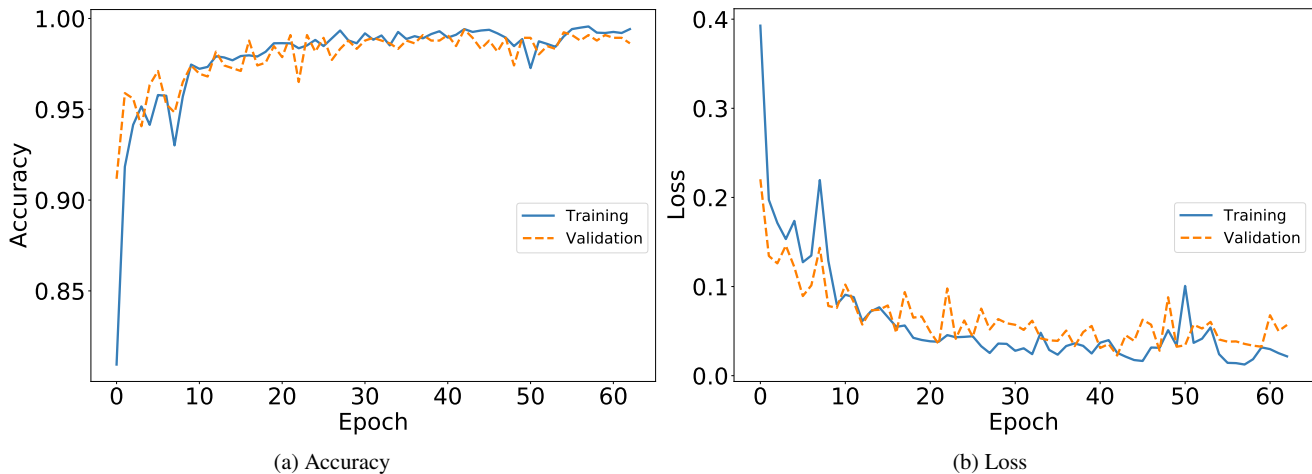


Fig. 7: Learning curves of the MeerCRAB3 model with  $T9$  and  $NRD$  as input. The left panel shows the training and validation accuracy over iterations/epochs. The right panel shows the change in negative log-likelihood/loss with epochs. It can be observed that the training objective decreases consistently over iterations, but at some point (around 48 epochs) the validation set loss eventually starts to increase again. An early-stopping technique is applied to avoid overfitting by terminating that training process. At this stage, the algorithm picks the best parameters at 48 epochs.

step increases the likelihood that the models will retain useful information and not be distracted by noise or spurious patterns.

As described above, the MeerLICHT database provides four images  $N$ ,  $R$ ,  $D$  and  $S$ . We perform several analyses which are presented in §4, where we use a combination of these images. This work allows us to understand which image/s is/are important for helping the CNN to output better classification results. We therefore use cut-outs of  $N$ ,  $R$ ,  $D$ ,  $S$  and stack them to form either of these input images:  $NRDS$  ( $30 \times 30 \times 4$ ),  $NRD$  ( $30 \times 30 \times 3$ ),  $NR$  ( $30 \times 30 \times 2$ ),  $D$  ( $30 \times 30 \times 1$ ), or  $S$  ( $30 \times 30 \times 1$ ).

Afterwards, we apply data augmentation to mitigate the risk of over-fitting which may result in poor generalisation performance upon data outside the training set. Therefore, at each training step, the images are augmented by flipping them randomly in a horizontal and/or vertical direction. We do not apply any rotation or translation to the images. This data augmentation step is important as it helps to increase the training sample size and the probability that the CNN models will encounter similar images twice, will decrease.

Moreover, to further avoid any over-fitting during training, we employ an early stopping technique to stop the training process if no further decrease in validation loss is observed for several epochs. The various cases and models are trained for a number of epochs varying from 40 to 150. We show the optimisation curves (the accuracy and loss curves) during training and validation in Figure 7 for the best models with  $NRD$  and  $T9$  as input. We observe that both the training and validation accuracy reaches a range between 98.5% to

Table 1: Contingency table used as a visual aid for model selection. The sum of A, B, C, and D represents the total number of instances in the test set. A is the number of instances correctly classified by both models. D is the number of instances misclassified by both models. B is the number of objects that model 1 correctly classified, but has been misclassified by model 2. C is the number of examples misclassified by model 1 but being correctly classified by model 2.

	Model 2 Correct	Model 2 Wrong
Model 1 Correct	A	B
Model 1 Wrong	C	D

99.5% where the algorithm picks the best parameters at 48 epochs.

### 3.1 Evaluation Performance

We use different evaluation techniques, for instance, the accuracy, the precision, the recall and the Matthew correlation coefficient (MCC) metrics to evaluate the MeerCRAB models. In addition, we utilize the McNemar test for model comparison.

#### 3.1.1 McNemar’s Test

The McNemar test (McNemar 1947) is a statistical test used to check marginal homogeneity in the context of statistical models. It is used to compare the predictive accuracy of two



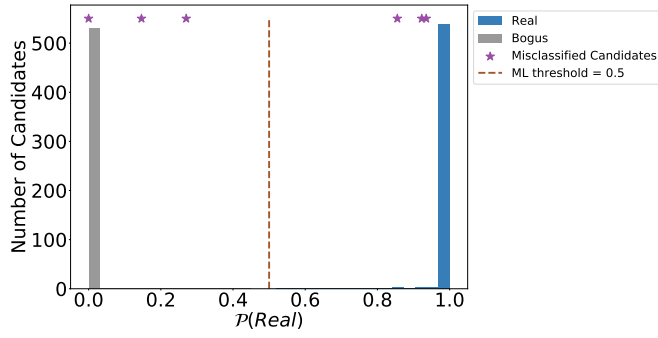


Fig. 8: Probability distribution on test data with 1095 candidates, trained with model configuration MeerCRAB3 with  $T9$  and  $NRD$  as input.

models' predictions and it is based on a contingency table as shown in Table 1. The latter provides insights for model selection, in contrast to a typical confusion matrix. It shows the number of instances/predictions model 1 and model 2 got right or wrong given a fixed test set. In McNemar's test, a null hypothesis,  $H_0$  is formulated such that  $\mathcal{P}(B)$  and  $\mathcal{P}(C)$  are similar or it can be interpreted as two models perform equally well. Therefore, the alternative hypothesis  $H_1$  is that  $\mathcal{P}(B) \neq \mathcal{P}(C)$  or the two models do not perform equally well. Edwards (1948) proposed a corrected McNemar test statistic that can be computed as given below:

$$\chi^2 = \frac{(|B - C| - 1)^2}{B + C}. \quad (4)$$

If the sum of B and C is greater than 25 or sufficiently large, under  $H_0$  the  $\chi^2$  value follows a chi-squared distribution with one degree of freedom. If we set a significance threshold for example,  $\alpha = 0.05$ , the p-value can be computed. Assuming that the null-hypothesis is true, the p-value implies the probability of observing a larger chi-squared value. However, if the p-value is less than  $\alpha$ , then the null hypothesis is rejected, that is, the two models do not perform equally well.

In the case where the sum of B and C is less than 25, an exact binomial test is used instead, since the chi-squared value may not be well approximated by the chi-squared distribution. Thus, the exact p-value is calculated as follows:

$$\text{p-value} = 2 \times \sum_{i=B}^n \binom{n}{i} 0.5^i (1 - 0.5)^{n-i}, \quad (5)$$

where  $n = B + C$  and a factor 2 indicates the computation of a two-sided p-value. For model selection, if the p-value is less than 0.05, we reject the null hypothesis, thus one model is outperforming the other. However, if the p-value is greater than 0.05, we do not reject the null hypothesis and it indicates that both models perform equally well.

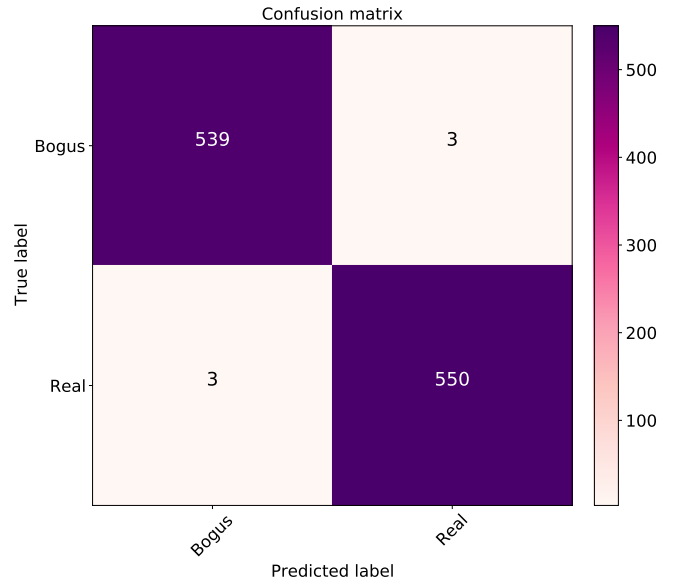


Fig. 9: Confusion Matrix without normalisation from a test set of 1095 candidates. The model is trained using MeerCRAB3 with  $T9$  and  $NRD$  as input. The diagonal represents the correctly classified instances in the test. The off-diagonals represent the number of instances that are misclassified. We note that we have a very low FP and FN with this model configuration.

#### 4 Results and Analysis

The classification performance of the MeerCRAB models are analysed as follows:

- The MeerCRAB models are trained on a subset sample of input images and validated on an unseen image sample.
- During the prediction phase, the trained models are then used to output probabilistic predictions for unseen images in the test set as shown in Figure 8. The probability distribution from the output of the MeerCRAB models spanned the range of  $P_{\text{MeerCRAB}} \in [0; 1]$ . Therefore, a candidate is predicted as bogus if  $P_{\text{MeerCRAB}} < 0.5$  and as real if  $P_{\text{MeerCRAB}} \geq 0.5$ .  $P_{\text{MeerCRAB}} = 0.5$  indicates a random guess and the MeerCRAB models are confused between real and bogus candidates.

We investigated various scenarios for training and evaluating the pipeline. We made use of three network structures: MeerCRAB1, MeerCRAB2, & MeerCRAB3. We also varied the number of images used as input to the three model architectures. We use these combinations of input images  $NRDS$ ,  $NRD$ ,  $NRS$ ,  $NR$ ,  $D$  and  $S$  independently. In addition, we investigated the effect of varying the thresholding applied on data labelling, i.e., the effect of noisy data labels as discussed in §2.2 and §2.3.

For all the experiments considered, it is worth mentioning that we train the networks with and without data augmenta-

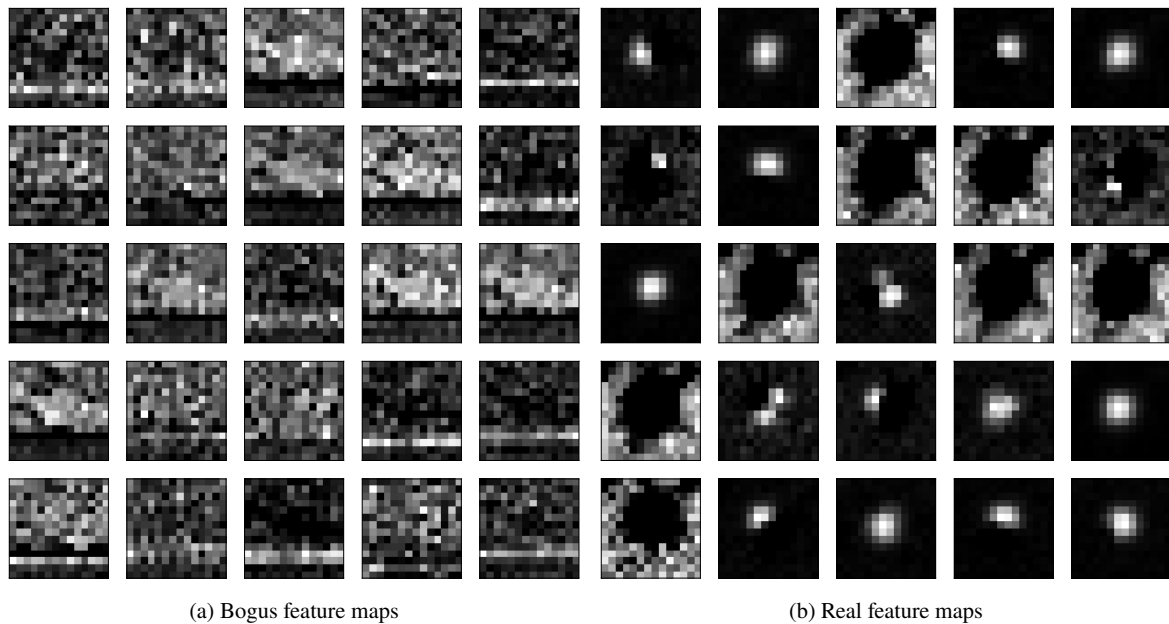


Fig. 10: Feature maps induced by the convolutional layer in MeerCRAB3 given a “bogus” and “real” source, respectively. We observe that the model distinguishes between background noise and the source at the center of an image.

tion. We found that employing data augmentation decreases the number of misclassifications. Therefore, we report results with the models trained with data augmentation only in this paper. Using data augmentation, we found the objective values steadily decreased during the fitting process on both the training set and validation set. Figure 7 provides an illustration of the objective functions and we observe that both the training and validation loss are close to each other, indicating that the models did not overfit on the training sample. Hence, the dropout layers as well as various regularization techniques used in the models are effective measures to prevent overfitting.

#### 4.1 Case studies

We start by providing an overall comparison of various scenarios used and will subsequently analyse some of the models along with certain modifications in more details. The MeerCRAB models are evaluated on various metrics. Based on the  $P_{\text{MeerCRAB}}$  value, we construct a confusion matrix to have an overview of the classification results. The confusion matrices display the fraction of correctly classified candidates as TP, TN along the diagonal. The off-diagonal values in the confusion matrices show the misclassified examples (FP and FN). We also evaluated the models based on precision, recall, accuracy, and MCC as discussed in §3.1. The results for the various scenario cases are summarised in Table 2, 3, 4, 5 and Figure 9.

##### 4.1.1 Data labelling based on Thresholding criteria

In supervised learning algorithms, the success of deep neural networks depends highly on the availability and accessibility of high-quality labelled training data. In this work, we found that the presence of label errors (label noise) in the training data greatly reduced the accuracy of all MeerCRAB models on test data. Unfortunately, large training datasets almost always contain examples with inaccurate or incorrect labels. It is a challenging task to train deep neural networks (DNNs) robustly with noisy labels (Han et al. 2018) as DNNs have a high capacity to fit noisy labels (Zhang et al. 2016), and this results in poorer model performance in practice.

In this paper, in order to sanity check the potential generalisation performance of our models, we utilised latent class models,  $L_{lcm}$  to label our data - including those samples for which vetters could not reach agreement. This approach allows us to introduce labelling noise. Whilst this noise reduces the performance of our models causing accuracy to drop to 0.968, it helps us obtain an impression of real-world performance where imperfect labelling and noise cannot be controlled for. Results show that models trained using such data still perform very well. This indicates that the networks are robust to noise.

Our analysis also involves comparing various thresholding criteria: **T8**, **T9**, and **T10** along with the MeerCRAB3 model with *NRD* as input. The results for labelling techniques are summarised in Table 2. We observe that as the threshold increased from **T8** to **T10**, the accuracy of the

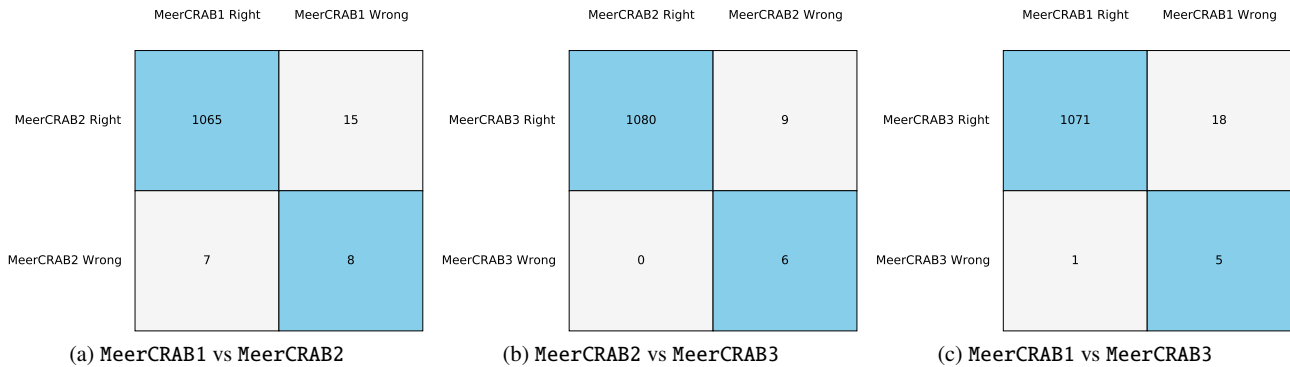


Fig. 11: The contingency tables for the three models under consideration with  $T9$  and  $NRD$  as input. For model selection, we compare the performance accuracy of each model on a similar test set. From the plots, we observe that MeerCRAB3 is a better model compared to MeerCRAB1 and MeerCRAB2.

model increases from 0.988 to 0.998 and MCC values increase from 0.976 to 0.995. However, when using the  $L_{lcm}$  method, we note a significant drop in  $L_{lcm}$  accuracy (0.968) as deep networks tend to memorize training label noise, resulting in poorer model performance. Therefore, it is necessary to obtain fairly high-quality labels for a CNN to work appropriately, thus removing noisy labelling from the model yields better model performance.

However, from here on we focus on experimentation that uses labels obtained via thresholding criteria :  $T9$  only, and not the  $L_{lcm}$ . we do this as we aim to have the best optimized model with an adequate number of candidates along with a good level of agreement on the labelling, such that we obtain fewer false positives and false negatives.

#### 4.1.2 Network architectures

We trained the MeerCRAB pipeline with three different architectures using  $T9$  data. MeerCRAB1 consists of a single  $CL$ , MeerCRAB2 is trained with 2  $CL$ s and MeerCRAB3 with 3  $CL$ s. From Table 3, Table 4 and Table 5, we note that MeerCRAB1 which is a shallow network yields a surprisingly good performance for  $T8$  to  $T10$ . Looking at Table 4 with  $T9$ , we note that MeerCRAB1 achieves an accuracy of 0.980 and  $MCC = 0.960$  on the test set. When using deeper networks (MeerCRAB2 and MeerCRAB3), we found that we obtain a better performance. The accuracy for MeerCRAB2 and MeerCRAB3 using  $NRD$  as input are 0.986 & 0.995 and  $MCC$  values are 0.973 & 0.989 respectively.

To have a better understanding of why MeerCRAB1 yields a good performance, we plot in Figure 10 the feature maps of the  $CL$  for a bogus and real example. We observe that there appears to be feature maps that activate on the background (“dark centre”), while other maps activate on different parts of the centre. This suggests that the network can distinguish

between the source itself and the background, thus it is able to classify images relatively unhindered by different levels of noise.

To determine which network performs best, we employ the McNemar statistical test as discussed in §3.1.1. We plot the contingency tables for the three models in Figure 11. The sample size in the B and C cells are relatively small and  $(B + C) < 25$  to approximate the chi-square value from the chi-square distribution. We therefore compute the p-value in this case from a binomial distribution. Assuming we use  $\alpha = 0.05$ , if the p-value is less than 0.05, we reject the null hypothesis that both models perform equally well on the test set and if the p-value is greater than 0.05, we do not reject the null hypothesis, we then conclude that the two models perform equally well. From Table 6, we note that when comparing MeerCRAB1 with MeerCRAB2, the p-values are greater than 0.05, we therefore conclude that the models have an equal performance. However, when comparing MeerCRAB1 with MeerCRAB3 and MeerCRAB2 with MeerCRAB3, the p-value is less than 0.05 this indicates that one model is performing better. When we analyse Figure 11(b,c), we note that MeerCRAB3 has less instances being misclassified compared to MeerCRAB1 and MeerCRAB2. Therefore, we conclude MeerCRAB3 is a better model compared to MeerCRAB1 and MeerCRAB2.

#### 4.1.3 Input Images

In this section, we investigate the effect of adding and removing images from the input to the CNN models. Vectors were shown only three images during vetting:  $N$ ,  $R$  and  $D$  images. However, when training and evaluating the three networks, we compare the different groups of images, to see whether a competitive performance can be achieved with more or less input data. Focusing on  $T9$  and MeerCRAB3,

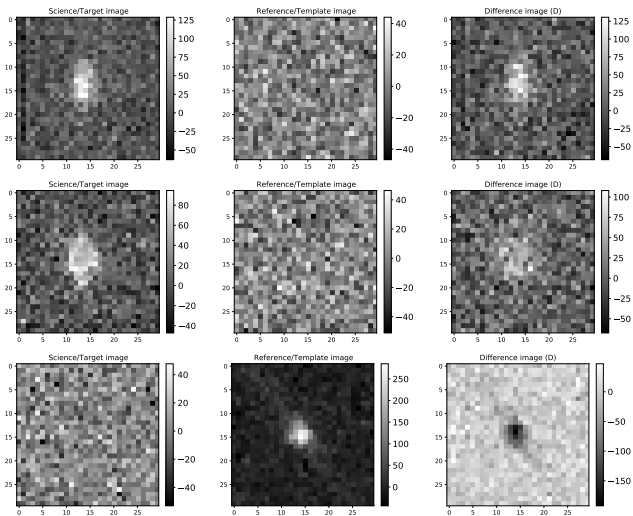


Fig. 12: The false positives obtained with MeerCRAB3, trained with  $T9$  labelling and  $NRD$  as input. These candidates are classified as bogus by humans. However, the best performing network misclassified them as real.

we note that  $NRD$  input yields the best performing model with an accuracy of 0.995 and MCC value of 0.989. Similar results are obtained with  $T8$  and  $T10$ . The second best model in  $T9$  is with input  $NRS$  yielding an accuracy of 0.990 and MCC value of 0.980. With only  $NR$  as input, we note that MeerCRAB3 performs equally well. Therefore, using a reduced image input set ( $NR$ ) yields a competitive performance and indicates that a reduced set of images is sufficient for separating real and bogus. However, we note that using only  $D$  or  $S$  as input worsens the classification performance and this indicates that using information only from the difference or significance imaging is insufficient.

## 4.2 Analysis of misclassification

With the various investigations, it is worth mentioning that the classification performance is, in general, very similar for the different MeerCRAB models, i.e., neither a particular network structure nor the involved parameters seem to have a significant influence on the final classification performance. The conclusion one can draw at this point is that a standard CNN model seems to be well-suited for the task at hand and that even relatively simple networks yield a performance that is competitive with state-of-the-art approaches.

In this section, we focus on our best model, MeerCRAB3 network with the  $NRD$  configuration and  $T9$  as input. In Figure 12 and Figure 13, we present all misclassifications it made.

In Figure 12, the top two rows show bogus candidates with the presence of elongated spikes but the CNN found high pixel values at the centre, thus got confused and classified

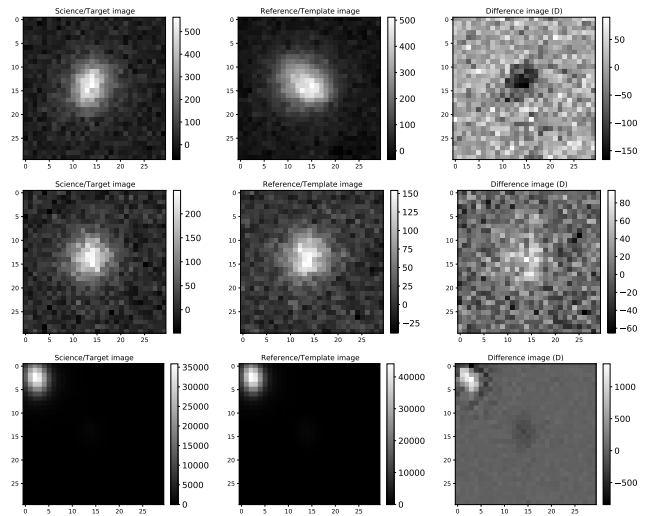


Fig. 13: The false negatives obtained with MeerCRAB3, trained with  $T9$  labelling and  $NRD$  as input. These candidates have been classified as real by vetters. However, the best model misclassified them as bogus candidates. The first two rows illustrate two real candidates with characteristics of an extended source with  $> 10$  pixels extent. The large extent of the sources can be attributed to that fact that the seeing can be very poor.

them as a real. The last row shows bogus candidates caused by blinking tail light of planes which can be recognized by the stripe. However, the MeerCRAB models seemingly recognized it as real due to the presence of a strong point source at the centre. However, we find that the decision made by MeerCRAB fulfils our requirements as we do not feed information related to elongated spikes and tail-light-trails when training the ML algorithm. These are not commonly occurring bogus events at present but may be added to our training set in the future and it will enable MeerCRAB to identify them.

Figure 13 shows real candidates being misclassified as bogus. The top two rows are likely to be real point sources because the Seeing can be very poor, thus leading to the large extent of  $> 10$  pixels. The fact that the source in the top row is oriented differently in the science/new and reference image suggests that it is not a Galaxy. However, these misclassifications are expected as these characteristics of real were not provided when training the network.

## 5 Conclusions

A deep learning framework, MeerCRAB, integrated in the MeerLICHT facility is a step forward in the automation and improvement of the transient vetting process. In practice, by using MeerCRAB we can significantly reduce the number of missed transients per night and this may have a great impact

on detecting and classifying the unknown unknowns of our universe.

In this paper, we detailed the process of developing MeerCRAB. To be able to train a deep neural network, we construct a large, high-quality labelled and representative dataset. To do so, we developed a vetting guidelines for vetters and taught them how real or bogus candidates in the MeerLICHT data appear. Then, a sample of 5000 candidates were provided to 10 vetters for labelling. Based on the vetters labels, we applied two methods to assign the final labelling to each candidate: (i) the *thresholding* method (**T8**, **T9** & **T10**) and (ii) latent class model  $L_{lcm}$ . At **T9**, a source is labelled as real if *atleast* 9 out of the 10 vetters labelled it as real or vice-versa. We found that **T9** is a good threshold criteria to be used since we have enough samples for training and testing the models, hence providing high quality labelled data. We found that going lower than this (i.e. **T7**, **T8**) or using  $L_{lcm}$ , added noisy labels. When used to train the network, such data decreased the performance of the models.

Moreover, we demonstrated that by increasing the depth of the network, (MeerCRAB1 to MeerCRAB3), the performance of the model increases as well. McNemar’s statistical test showed that MeerCRAB3 performs better than MeerCRAB1 and MeerCRAB2. In addition, we used a combination of input images (new ( $N$ ), reference ( $R$ ), difference ( $D$ ), significance ( $S$ )) as input to the three networks. We found that with only  $NR$ , we obtained competitive results. We also observed that adding the difference and significance images improves network performance.

In summary the best performing model has the following configuration: **T9** with MeerCRAB3 having  $NRD$  as input. This model yields an accuracy of 99.5 % and MCC value of 0.989. This performance achieves an acceptable false positive and false negative rate for the real-time MeerLICHT transient detection pipeline requirements.

MeerCRAB is a crucial component of the MeerLICHT project which aims to detect and identify transient and variable sources. With the streaming data coming from MeerLICHT, the vast majority of astrophysical data are not only challenging to store, but also to classify efficiently and effectively. Therefore, MeerCRAB will enable the rapid identification of promising astrophysical sources in timely-manner. In addition, MeerCRAB can be adapted to be a system that disentangles interesting objects from a noisy background. We have already implemented similar models in radio astronomy that distinguish Single Pulses from Radio Frequency Interference for the MeerKAT telescope (FRBID<sup>7</sup>: Fast Radio Burst Intelligent Distinguisher). MeerCRAB is a flexible software system, thus we were able to easily modify it to integrate different images as its inputs and as result, achieved high levels of performance when using it for radio astronomy

Table 2: The results for various labelling methods are presented in terms of precision, recall, accuracy and MCC values using  $NRD$  as input to the three models.

Methods of labelling	Precision	Recall	Accuracy	MCC
MeerCRAB1				
$L_{lcm}$	0.96	0.96	0.960	0.920
T8	0.98	0.98	0.980	0.958
T9	0.98	0.98	0.979	0.958
T10	0.99	0.99	0.991	0.983
MeerCRAB2				
$L_{lcm}$	0.97	0.97	0.967	0.936
T8	0.99	0.98	0.977	0.953
T9	0.99	0.99	0.986	0.973
T10	0.99	0.99	0.994	0.988
MeerCRAB3				
$L_{lcm}$	0.97	0.97	0.968	0.936
T8	0.99	0.99	0.988	0.976
<b>T9</b>	<b>0.99</b>	<b>0.99</b>	<b>0.995</b>	<b>0.989</b>
T10	1.00	1.00	0.998	0.995

Table 3: The results with Threshold 8 (**T8**) are presented in terms of precision, recall, accuracy and MCC values using various combinations of input images (new ( $N$ ), reference ( $R$ ), difference ( $D$ ), and significance ( $S$ )) to the three models.

Number of Images	Precision	Recall	Accuracy	MCC
MeerCRAB1				
NRDS	0.98	0.98	0.980	0.958
NRD	0.98	0.98	0.977	0.954
NRS	0.97	0.97	0.971	0.942
NR	0.96	0.96	0.962	0.923
D	0.88	0.88	0.877	0.762
S	0.83	0.83	0.831	0.662
MeerCRAB2				
NRDS	0.97	0.97	0.975	0.948
NRD	0.98	0.98	0.977	0.953
NRS	0.99	0.99	0.986	0.973
NR	0.99	0.99	0.987	0.975
D	0.91	0.91	0.910	0.825
S	0.89	0.89	0.887	0.777
MeerCRAB3				
NRDS	0.98	0.98	0.983	0.966
NRD	<b>0.99</b>	<b>0.99</b>	<b>0.988</b>	<b>0.976</b>
NRS	0.98	0.98	0.983	0.968
NR	0.98	0.98	0.981	0.963
D	0.92	0.92	0.921	0.843
S	0.89	0.89	0.891	0.786

images. Given the performance of MeerCRAB on both optical and radio image sources in astronomy, the method may have utility for those working in related areas.

## 6 Declarations

### Funding

ZH acknowledges support from the UK Newton Fund as part of the Development in Africa with Radio Astronomy

<sup>7</sup> See [https://github.com/Zafirah13/multi\\_input\\_frbid](https://github.com/Zafirah13/multi_input_frbid) and <https://github.com/Zafirah13/FRBID>

Table 4: The results with Threshold 9 (**T9**) are presented in terms of precision, recall, accuracy and MCC values using various combinations of input images (new (*N*), reference (*R*), difference (*D*), and significance (*S*)) to the three models.

Number of Images	Precision	Recall	Accuracy	MCC
<b>MeerCRAB1</b>				
NRDS	0.98	0.98	0.980	0.960
NRD	0.98	0.98	0.979	0.958
NRS	0.98	0.98	0.978	0.956
NR	0.97	0.97	0.972	0.946
D	0.86	0.83	0.823	0.690
S	0.86	0.85	0.853	0.708
<b>MeerCRAB2</b>				
NRDS	0.99	0.99	0.988	0.976
NRD	0.99	0.99	0.986	0.973
NRS	0.99	0.99	0.986	0.973
NR	0.99	0.99	0.989	0.978
D	0.91	0.91	0.912	0.827
S	0.89	0.87	0.865	0.751
<b>MeerCRAB3</b>				
NRDS	0.99	0.99	0.987	0.974
NRD	<b>0.99</b>	<b>0.99</b>	<b>0.995</b>	<b>0.989</b>
NRS	0.99	0.99	0.990	0.980
NR	0.99	0.99	0.989	0.978
D	0.93	0.93	0.931	0.863
S	0.89	0.87	0.868	0.760

Table 5: The results with Threshold 10 (**T10**) are presented in terms of precision, recall, accuracy and MCC values using various combinations of input images (new (*N*), reference (*R*), difference (*D*), and significance (*S*)) to the three models.

Number of Images	Precision	Recall	Accuracy	MCC
<b>MeerCRAB1</b>				
NRDS	1.00	1.00	0.995	0.990
NRD	0.99	0.99	0.991	0.983
NRS	0.98	0.98	0.985	0.970
NR	0.99	0.99	0.986	0.973
D	0.92	0.92	0.920	0.841
S	0.93	0.93	0.934	0.868
<b>MeerCRAB2</b>				
NRDS	1.00	1.00	0.995	0.990
NRD	0.99	0.99	0.994	0.988
NRS	0.98	0.98	0.984	0.968
NR	0.99	0.99	0.992	0.985
D	0.94	0.94	0.944	0.888
S	0.94	0.94	0.940	0.881
<b>MeerCRAB3</b>				
NRDS	0.99	0.99	0.990	0.980
NRD	<b>1.00</b>	<b>1.00</b>	<b>0.998</b>	<b>0.995</b>
NRS	0.99	0.99	0.994	0.988
NR	0.99	0.99	0.985	0.970
D	0.94	0.94	0.939	0.878
S	0.94	0.94	0.943	0.886

Table 6: McNemar’s Test using *T9* and *NRD* results for model selection. MeerCRAB3 has the best performance than MeerCRAB1 and MeerCRAB2 as the p-value is less than 0.05.

Models	P-value
MeerCRAB1 vs MeerCRAB2	0.13400
MeerCRAB2 vs MeerCRAB3	0.00390
MeerCRAB1 vs MeerCRAB3	0.00008

(DARA) Big Data project delivered via the Science & Technology Facilities Council (STFC). BWS acknowledges funding from the European Research Council (ERC) under the European Union’s Horizon 2020 research and innovation programme (grant agreement No. 694745). PJG and SDW are supported by NRF SARChI Grant 111692.

### Conflicts of interest/Competing interests

Not applicable

### Availability of data and material

Data will be available upon request.

### Code availability

MeerCRAB code and pre-trained models are available on Github at <https://github.com/Zafirah13/meercrab> and on Zenodo at <https://doi.org/10.5281/zenodo.4049943>.

### Acknowledgements

We thank the referee for useful comments and suggestions for improving this paper. We would like to thank the people who gave up their time to do the vetting of the sample: Laura Driessen, Naomi titus, Mark Beijer, Nadia Blagorodnova, Joris Kersten, David Modiano and Roque Ruiz Carmona, without whose effort this work would not have been possible. We would like to also thank Arrykrishna Mootoovaloo and Fabian Gieseke for useful discussion. The MeerLICHT consortium is a partnership between Radboud University, the University of Cape Town, the Netherlands Organisation for Scientific Research (NWO), the South African Astronomical Observatory (SAAO), the University of Oxford, the University of Manchester and the University of Amsterdam, in association with and, partly supported by, the South African Radio Astronomy Observatory (SARAO), the European Research Council and the Netherlands Research School for Astronomy (NOVA).

## References

- Agarap, A. F., Deep Learning using Rectified Linear Units (ReLU). 2018, *arXiv e-prints*, [arXiv:1803.08375](https://arxiv.org/abs/1803.08375)
- Bellm, E. C., Kulkarni, S. R., Graham, M. J., et al., The Zwicky Transient Facility: System Overview, Performance, and First Results. 2019, *PASP*, **131**, 018002
- Bertin, E. 2011, in *Astronomical Society of the Pacific Conference Series*, Vol. 442, *Astronomical Data Analysis Software and Systems XX*, ed. I. N. Evans, A. Accomazzi, D. J. Mink, & A. H. Rots, **435**
- Bertin, E. & Arnouts, S., SExtractor: Software for source extraction. 1996, *A&AS*, **117**, 117
- Bloemen, S., Groot, P., Woudt, P., et al. 2016, in *Society of Photo-Optical Instrumentation Engineers (SPIE) Conference Series*, Vol. 9906, *Proc. SPIE*, **990664**
- Cabrera-Vives, G., Reyes, I., Förster, F., Estévez, P. A., & Maureira, J.-C., Deep-HiTS: Rotation Invariant Convolutional Neural Network for Transient Detection. 2017, *ApJ*, **836**, 97
- Chollet, F. & others. 2018, Keras: The Python Deep Learning library
- Drake, A. J., Djorgovski, S. G., Mahabal, A., et al., First Results from the Catalina Real-Time Transient Survey. 2009, *ApJ*, **696**, 870
- Edwards, A. L., Note on the “correction for continuity” in testing the significance of the difference between correlated proportions. 1948, *Psychometrika*, **13**, 13
- Formann, A. K. 1984, *Die latent-class-analyse: Einführung in Theorie und Anwendung* (Beltz)
- Gaia Collaboration, Brown, A. G. A., Vallenari, A., et al., Gaia Data Release 1. Summary of the astrometric, photometric, and survey properties. 2016, *A&A*, **595**, A2
- Gieseke, F., Bloemen, S., van den Bogaard, C., et al., Convolutional neural networks for transient candidate vetting in large-scale surveys. 2017, *MNRAS*, **472**, 3101
- Groot, P. J., The multi-colour dynamic Universe explored. 2019, *Nature Astronomy*, **3**, 1160
- Han, B., Yao, Q., Yu, X., et al., Co-teaching: Robust Training of Deep Neural Networks with Extremely Noisy Labels. 2018, *arXiv e-prints*, [arXiv:1804.06872](https://arxiv.org/abs/1804.06872)
- Hosenie, Z., Lyon, R., Stappers, B., Mootoovaloo, A., & McBride, V., Imbalance learning for variable star classification. 2020, *MNRAS*, **493**, 6050
- Hosenie, Z., Lyon, R. J., Stappers, B. W., & Mootoovaloo, A., Comparing Multiclass, Binary, and Hierarchical Machine Learning Classification schemes for variable stars. 2019, *MNRAS*, **488**, 4858
- Jonas, J. & MeerKAT Team. 2016, in *MeerKAT Science: On the Pathway to the SKA*, **1**
- Kaiser, N., Burgett, W., Chambers, K., et al. 2010, in *Society of Photo-Optical Instrumentation Engineers (SPIE) Conference Series*, Vol. 7733, *Proc. SPIE*, **77330E**
- Keller, S. C., Schmidt, B. P., Bessell, M. S., et al., The SkyMapper Telescope and The Southern Sky Survey. 2007, *Publ. Astron. Soc. Australia*, **24**, 1
- Kingma, D. P. & Ba, J., Adam: A Method for Stochastic Optimization. 2014, *arXiv e-prints*, [arXiv:1412.6980](https://arxiv.org/abs/1412.6980)
- Lang, D., Hogg, D. W., Mierle, K., Blanton, M., & Roweis, S., Astrometry.net: Blind Astrometric Calibration of Arbitrary Astronomical Images. 2010, *AJ*, **139**, 1782
- Lecun, Y., Haffner, P., Bottou, L., & Bengio, Y., Object Recognition with Gradient-Based Learning. 1999
- Lin, H., Li, X., & Zeng, Q., Pulsar Candidate Sifting Using Multi-input Convolution Neural Networks. 2020, *arXiv e-prints*, [arXiv:2007.14843](https://arxiv.org/abs/2007.14843)
- LSST Science Collaboration, Abell, P. A., Allison, J., et al., LSST Science Book, Version 2.0. 2009, *arXiv e-prints*, [arXiv:0912.0201](https://arxiv.org/abs/0912.0201)
- McCutcheon, A. L. 1987, *Latent class analysis* No. 64 (Sage)
- McNemar, Q., Note on the sampling error of the difference between correlated proportions or percentages. 1947, *Psychometrika*, **12**
- Muthukrishna, D., Narayan, G., Mandel, K. S., Biswas, R., & Hložek, R., RAPID: Early Classification of Explosive Transients Using Deep Learning. 2019, *PASP*, **131**, 118002
- Paterson, K. 2019, in *IAU Symposium*, Vol. 339, *Southern Horizons in Time-Domain Astronomy*, ed. R. E. Griffin, **203–203**
- Rau, A., Kulkarni, S. R., Law, N. M., et al., Exploring the Optical Transient Sky with the Palomar Transient Factory. 2009, *PASP*, **121**, 1334
- Richards, J. W., Starr, D. L., Butler, N. R., et al., On Machine-learned Classification of Variable Stars with Sparse and Noisy Time-series Data. 2011, *ApJ*, **733**, 10
- Shappee, B. J., Prieto, J. L., Grupe, D., et al., The Man behind the Curtain: X-Rays Drive the UV through NIR Variability in the 2013 Active Galactic Nucleus Outburst in NGC 2617. 2014, *ApJ*, **788**, 48
- Vafaei Sadr, A., Vos, E. E., Bassett, B. A., et al., DEEPSOURCE: point source detection using deep learning. 2019, *MNRAS*, **484**, 2793
- van Dokkum, P. G., Cosmic-Ray Rejection by Laplacian Edge Detection. 2001, *PASP*, **113**, 1420
- Zackay, B., Ofek, E. O., & Gal-Yam, A., Proper Image Subtraction-Optimal Transient Detection, Photometry, and Hypothesis Testing. 2016, *ApJ*, **830**, 27
- Zhang, C., Bengio, S., Hardt, M., Recht, B., & Vinyals, O., Understanding deep learning requires rethinking generalization. 2016, *arXiv e-prints*, [arXiv:1611.03530](https://arxiv.org/abs/1611.03530)